HHS Public Access

Author manuscript

Biol Psychiatry. Author manuscript; available in PMC 2022 July 06.

Published in final edited form as:

Biol Psychiatry. 2021 February 01; 89(3): 256–269. doi:10.1016/j.biopsych.2020.07.014.

Neurogranin, encoded by the schizophrenia risk gene *NRGN*, bidirectionally modulates synaptic plasticity via calmodulin-dependent regulation of the neuronal phosphoproteome

Hongik Hwang[1,3,7,*], **Matthew J. Szucs**[5,†], **Lei J. Ding**[1,4,†], **Andrew Allen**[5], **Xiaobai Ren**[1], **Henny Haensgen**[1], **Fan Gao**[1], **Hyewhon Rhim**[7,8], **Arturo Andrade**[6], **Jen Q. Pan**[5], **Steven A. Carr**[5], **Rushdy Ahmad**[5], **Weifeng Xu**[1,2,*,‡]

[1]Picower Institute for Learning and Memory, Massachusetts Institute of Technology, Cambridge, MA 02139, USA.

[2]Department of Brain and Cognitive Sciences, Massachusetts Institute of Technology, Cambridge, MA 02139, USA.

[3]Department of Chemistry, Massachusetts Institute of Technology, Cambridge, MA 02139, USA.

[4]Department of Biology, Massachusetts Institute of Technology, Cambridge, MA 02139, USA.

[5]Broad Institute of MIT and Harvard, Cambridge, MA 02139, USA.

[6]Department of Biological Sciences, University of New Hampshire, Durham, NH 03824, USA.

[7]Center for Neuroscience, Brain Science Institute, Korea Institute of Science and Technology (KIST), Seoul 02792, Republic of Korea.

[8]Division of Bio-Medical Science & Technology, KIST School, Korea University of Science and Technology, Seoul 02792, Republic of Korea.

Abstract

Background: Neurogranin (Ng), encoded by the schizophrenia risk gene *NRGN*, is a calmodulin-binding protein enriched in the postsynaptic compartments, and its expression is

[*]Corresponding authors: Hongik Hwang, Ph.D. Center for Neuroscience Brain Science Institute, Korea Institute of Science and Technology (KIST), 5 Hwarang-ro 14-gil, Seongbuk-gu, L7305, Seoul 02792, Republic of Korea, hongik@mit.edu (H.H.), Weifeng Xu, Ph.D., Carney Institute for Brain Science, Department of Neuroscience, Brown University, Sidney Frank Hall, 185 Meeting Street, Box G-LN, Providence, RI 02912, USA, weifeng_xu@brown.edu (W.X.).

[‡]Present address: Carney Institute for Brain Science, Department of Neuroscience, Brown University, Providence, RI 02912, USA.

[†]These authors contributed equally to this work.

Author responsibilities were as follows: Conceptualization, H.H. and W.X.; Methodology, H.H., A.A.[5], X.R., H.H.[1], J.Q.P., S.A.C., R.A. and W.X.; Investigation, H.H., M.J.S., A.A.[5] and W.X.; Formal Analysis, H.H., L.J.D., A.A.[5], F.G., A.A.[6], R.A. and W.X.; Writing – Original Draft, H.H., R.A. and W.X.; Writing – Review & Editing, H.H., A.A.[6], R.A. and W.X.; Funding Acquisition, H.R. and W.X.; Supervision, H.R., J.P.Q., S.A.C., R.A. and W.X.

Disclosures

We would like to thank Y. Liu for her excellent technical support, Dr. Hector De Jesus-Cortes for his help with western blotting, and Drs. E. Scolnick, E. Nedivi, L.-H. Tsai, M. Bear, J. Lisman and M. Wilson for their comments.

The authors report no biomedical financial interests or potential conflicts of interest.

reduced in the post-mortem brains of schizophrenic patients. Experience-dependent translation of Ng is critical for encoding contextual memory, and Ng regulates the developmental plasticity in the primary visual cortex during the critical period. However, the overall impact of Ng on the neuronal signaling that regulates synaptic plasticity is unknown.

Methods: Altered Ng expression was achieved via virus-mediated gene manipulation in mice. The effect on long-term potentiation (LTP) was accessed using spike-timing-dependent plasticity protocols. Quantitative phosphoproteomics analyses led to discoveries in significant phospho-targets. An identified candidate was examined with high-throughput planar patch clamp, and validated with pharmacological manipulation.

Results: Ng bidirectionally modulated LTP in the hippocampus. Decreasing Ng levels significantly affected the phosphorylation pattern of postsynaptic density proteins, including glutamate receptors, GTPases, kinases, RNA binding proteins, selective ion channels and ionic transporters, some of which highlighted the clusters of schizophrenia- and autism-related genes. Hypo-phosphorylation of NMDAR subunit Grin2A, one significant phospho-target, resulted in accelerated decay of NMDAR currents. Blocking protein phosphatase PP2B activity rescued the accelerated NMDAR current decay and the impairment of LTP mediated by Ng knockdown, implicating the requirement of synaptic PP2B activity for the deficits.

Conclusions: Altered Ng levels affect the phosphorylation landscape of neuronal proteins. PP2B activity is required for mediating the deficit in synaptic plasticity caused by decreasing Ng levels, revealing a novel mechanistic link of a schizophrenia risk gene to cognitive deficits.

Keywords

Neurogranin; Synaptic plasticity; Hippocampus; NMDA receptor; Phosphoproteome; Schizophrenia

Introduction

Schizophrenia is one of the leading causes of disability worldwide, and affected individuals suffer from hallucinations, delusions, and cognitive dysfunction (1–3). The highly heritable nature of schizophrenia implies genetic underpinnings (4, 5), but the exact pathophysiology remains unknown. Over 100 genetic loci are associated with schizophrenia (6–14), and neurogranin (Ng, gene: *NRGN*) is identified as a risk gene in multiple populations (6, 7, 15–17). Individuals carrying the *NRGN* risk variant exhibit decreased hippocampal activation during contextual learning (18). High-risk haplotype lowered *NRGN* expression compared to the protective haplotype (19), and Ng immunoreactivity was reduced in the prefrontal cortex regions in schizophrenia patients (20), implicating Ng hypofunction in schizophrenia.

Ng levels are dynamically regulated during development under different environmental and behavioral states (21–24). In the primary visual cortex, Ng starts to express postnatally and reaches plateau during the critical period of the ocular dominance plasticity (25). In adult mice, novel experience enhances Ng expression in the hippocampus, which is required for contextual memory formation (26). Given this observation, hypofunction of Ng may induce experience-dependent developmental deficit in excitatory synapse connectivity or cognitive impairment.

Ng is highly expressed in the postsynaptic compartment of principal neurons in the cerebral cortex, hippocampus (22, 23), and binds to calmodulin (CaM) via the IQ (isoleucine-glutamine) domain, suggesting the role of Ng in controlling Ca^{2+}/CaM-dependent neuronal functions (27, 28). The relative activation of Ca^{2+}/CaM-dependent protein kinase II (CaMKII) and protein phosphatase 2B (PP2B, calcineurin) upon N-methyl-D-aspartate (NMDA) receptor activation determines the direction of long-term potentiation (LTP) and long-term depression (LTD), the substrate for learning and memory (29–39). While this CaMKII/PP2B axis of synaptic regulation is presumably embedded in a more intricate signaling complex (40), its role in synaptic plasticity is in accordance with the push-pull mechanism controlling the directionality and efficacy of synaptic plasticity (41–43). PP2B is preferentially activated when CaM is limited due to its higher affinity for Ca^{2+}/CaM. CaMKII is abundant in the postsynaptic compartment, accumulates at the synapses upon tetanic stimulation (44), and becomes constitutively active upon autophosphorylation (45–49), after sufficient Ca^{2+}/CaM-dependent activation (50–52). Therefore, the expression of synaptic plasticity is highly sensitive to CaM availability, and Ng was proposed to control synaptic plasticity by regulating Ca^{2+}/CaM dynamics at excitatory synapses (Figure 1A) (53–56). While previous studies examined the role of Ng in synaptic plasticity, the results varied depending on the use of different mouse lines, slice preparations, or animal ages (57, 58), implicating that the developmental stage and basal neural activity influence the effect of Ng on synaptic plasticity.

Here, we used lentiviral-mediated gene transfer to manipulate Ng levels, and examined its influence on synaptic plasticity. Given the potential impact of Ng levels on Ca^{2+}/CaM-dependent signaling, we adapted quantitative phosphoproteomic analysis to identify targets downstream from Ng that regulate synaptic plasticity. From our results, we propose an Ng-PP2B-NMDAR axis as a potential therapeutic target for cognitive impairment associated with schizophrenia.

Methods and Materials

Essential methods and materials are described below, and detailed information can be found in Supplemental Methods and Materials.

Animal Care

7–9 weeks old male C57BL/6 mice (Charles River, USA) were used in electrophysiology. All mice were housed in a temperature-controlled animal facility at Massachusetts Institute of Technology (MIT) or at Korea Institute of Science and Technology (KIST), and were given *ad libitum* access to food and water. All procedures related to animal and treatment conformed to the Guide for the Care and Use of Laboratory Animals and were approved by the Committee on Animal Care of MIT and by the Institutional Animal Care and Use Committee of KIST.

Cell Cultures

Dissociated cortical neuron culture was prepared from newborn pups of C57BL/6 mice using established protocols (26, 59). Constructs for expressing NMDAR subunits

were co-transfected with FLP recombinase (ThermoFisher) into Flp-In T-REx 293 cells (ThermoFisher) and selected for hygromycin resistance. HEK cells were used for high-throughput planar patch clamp with the SyncroPatch 384PE system (60).

Molecular Cloning

The lentiviral transfer vectors FUGW and FHUGW were used to create lentiviral constructs used in this study (61, 62). Rat Grin1 was cloned downstream of its 31 amino acid signal peptide and EGFP in frame with a P2A peptide fused to rat Grin2A.

Immunoblot Analysis

Cortical neuron culture infected with lentivirus was subjected to immunoblot analysis for lentivirus characterization (59, 61). For analyzing phosphorylated protein with Phos-Tag, a separating gel prepared with Phos-Tag acrylamide was used (63, 64). In pull-down assay, HEK cells transiently transfected with a plasmid expressing wild-type Ng or mutant Ng lacking CaM-binding IQ motif were used.

Live-Cell Imaging

HEK cells were plated on glass bottom 35-mm tissue culture dishes (MatTek) and induced for two days with doxycycline (Dox). Cells were maintained in a stage top incubator (Okolab) at 37°C and 5% CO_2 and imaged with a CSU-X1 spinning disc confocal (Andor).

Stereotaxic Surgery and Slice Physiology

7-week-old mice were anesthetized with a ketamine/xylazine cocktail by intraperitoneal injection. After confirming anesthesia, lentivirus was injected into the hippocampus based on the antero-posterior and lateral coordinates assigned to the CA1 region (AP: −2.0 mm, ML: ±1.5 mm, DV: −1.4 mm). Following the injection, mice were returned to their cages and allowed to recover. All experiments were performed 5–9 days after injection. Acute hippocampal slices (300-μm thick) were prepared based on a published protocol (65).

Proteome and Phosphoproteome Study

Neuron cultures were lysed in urea with protease and phosphatase inhibitors. The protocols for subsequent digestion, sample processing and data analyses are detailed in Supplemental Methods and Materials (66–74).

Statistical analysis

The sample size was chosen based on published studies in the field, and no statistical methods were used to predetermine the sample size. All bar graphs are presented as the mean ± standard error of the mean (SEM). The sample size and statistical methods used in each experiment is provided in the relevant figure legends. All statistical analysis was conducted using GraphPad Prism (GraphPad Software), and significance is shown as $*p<0.05$, $**p<0.01$, $***p<0.001$.

Results

Ng overexpression broadens the timing window for spike-timing-dependent LTP via direct interaction with CaM

The overexpression of Ng-GFP was achieved using lentivirus and confirmed by western blot in neuron culture (Ng OE, Figure 1B, C). The band intensity of Ng-GFP in Ng OE was ~170% of the endogenous Ng (Supplemental Figure S1). Acute hippocampal slices were prepared 5–9 days after injecting the lentivirus in the CA1 region (Figure 1D). Both paired-pulse ratio (PPR) and AMPAR/NMDAR ratio (A/N ratio) were not significantly different between infected and uninfected neurons from the same animals (Figure 1E, F), indicating that Ng OE does not alter presynaptic release probability and basal synaptic transmission at SC-CA1 synapses. Moreover, stimulation intensity and the corresponding basal excitatory postsynaptic potentials (EPSPs) were not different between infected and uninfected neurons (Supplemental Figure S2), further supporting that Ng manipulation does not affect basal transmission.

The effect of Ng OE on synaptic plasticity was examined using the spike-timing-dependent plasticity (STDP) protocol, in which the timing between pre- and postsynaptic stimulations controls plasticity (75–77). To induce STDP-LTP, a pairing consisted of presynaptic stimulation followed by action potentials was repeated 100 times (Figure 1G). When the pairing was performed at a 10-ms interval, both uninfected and infected neurons expressed robust LTP with a similar degree (Figure 1H-K), indicating that Ng OE exerts no additional effects on the magnitude of LTP. We then tested a less optimal interval, 20 ms, driving less cooperated activity at SC-CA1 synapses. This pairing protocol no longer induced LTP in uninfected neurons (Figure 2A, G, H); whereas neurons with Ng OE robustly expressed LTP (Figure 2B, G, H), indicating that increased Ng levels broadened the temporal association window for STDP-LTP.

To test whether this effect is mediated by the interaction between Ng and CaM, we created an Ng mutant without the IQ motif (Figure 2C, D, NgΔIQ). Using the pull-down assay with CaM beads, we confirmed that wild-type Ng preferentially binds CaM under low calcium (EGTA), while NgΔIQ does not interact with CaM (Figure 2E). As expected, NgΔIQ OE did not trigger LTP by the induction protocol with a 20-ms interval (Figure 2F-H), indicating that CaM-Ng interaction is required to promote STDP-LTP by Ng OE.

Ng knockdown abolishes the induction of STDP-LTP at SC-CA1 synapses

We next examined whether the Ng-dependent modulation of STDP-LTP is bidirectional. A lentiviral vector was constructed to knockdown Ng (Figure 3A, Ng KD), and the knockdown was highly effective 7–10 days after infection in neuron culture (Figure 3B, control bands are the same as Figure 1C). Similar to Ng OE, Ng KD did not affect PPR and A/N ratio at SC-CA1 synapses (Figure 3C, D). The effect of Ng KD on STDP-LTP was examined using the protocol with a 10-ms interval, and LTP was completely abolished in neurons with Ng KD (Figure 3E-H), indicating the essential role of Ng for STDP-LTP.

We further examined the effect of Ng on STDP-LTD using an inverted induction protocol (Supplemental Figure S3A). When the pairing was performed with the 10-ms interval, both

control and Ng KD neurons displayed robust LTD (Supplemental Figure S3B-E), whereas the same protocol triggered strong LTP in Ng OE neurons (Supplemental Figure S4). Together, these results implicate that elevated Ng levels broaden the timing window for STDP-LTP expression, and reduced Ng levels prevent LTP.

Decreased Ng levels affect the phosphorylation pattern in the postsynaptic phosphoproteome, inducing hypo-phosphorylation of NMDAR subunit Grin2A

Given the role of Ng in regulating CaM availability, we hypothesized that Ng KD influences the activation of Ca^{2+}/CaM-dependent kinases and phosphatases, thereby leading to a global change in phosphoproteome, including targets affecting synaptic plasticity. To test this idea, phosphopeptides were enriched from cell lysates of neuronal culture infected with GFP or Ng KD lentivirus, and total proteome and phosphoproteome were analyzed using quantitative mass spectrometry (Figure 4A) (78, 79).

In the proteomic dataset, Ng levels were significantly reduced by Ng KD to 12%, confirming the effective knockdown (Supplemental Table S1). To analyze the effect of Ng KD on total protein expression, we performed the Gene Ontology analysis using Enrichr (80, 81). General cellular functions, rather than neuronal specific processes, were highlighted in the top ten processes in both categories (Supplemental Figure S5). The levels of Calm1, the only CaM gene identified, were not significantly different between control and Ng KD. Similarly, no significant differences were detected in CaMKIIα, β, δ, γ, all PP2A catalytic subunits, and PP2B catalytic isoforms α, γ. There is a small but significant decrease of the PP2B catalytic isoform β, to 80% of the control levels. The expression of CaM, PP2B (catalytic and regulatory subunits), CaMKII and CaMKII phosphorylation at T286 were confirmed unaffected by Ng KD using western blot (Supplemental Figure S6), together implicating that the influence of Ng KD on the protein levels of the core CaMKIIα/PP2B enzymes is limited.

The phosphoproteome data were normalized to the total proteome when proteins were confidently identified in the total proteome dataset (Supplemental Table S2). Un-normalized P-sites were omitted from subsequent analysis. Near 30,000 phosphorylation sites (P-sites) comprising of 5,485 proteins were analyzed, and 4,744 (~16%) of these P-sites derived from 2,413 proteins exhibited a significant change in their phosphorylation status compared to control (Figure 4B, FDR≤0.05). Using the hypergeometric test, we found that differentially regulated P-sites were significantly over-represented in the set of known postsynaptic density (PSD) proteins ($p<2\times10^{-11}$, Supplemental Table S3) (73). Specifically, 27% and 26% of the proteins with up- and down-regulated P-sites overlapped with the PSD proteomic dataset, respectively (Supplemental Table S3), indicating that Ng KD altered the phosphorylation pattern of postsynaptic components considerably. We further performed GO enrichment analysis (82, 83), separately on the sets of up- and down-phosphorylated PSD proteins (74). Notably, overlapping and distinct pathways were highlighted in both up- and down-regulated clusters (Figure 4C), which was also observed with pathway analysis using synaptic GO (SynGO) (84). Both up- and down-regulated gene sets highlighted organization, presynaptic and signaling processes. Genes containing up-regulated P-sites exhibited higher significance in chemical synaptic transmission and vesicle cycling,

whereas those containing down-regulated P-sites exhibited higher significance in structural constituents of synapse (Supplemental Figure S7).

Given the association of Ng with autism spectrum disorders (ASDs) and schizophrenia, and the convergence of glutamatergic synaptic components in ASDs and schizophrenia, we tested whether the changes in phosphoproteome overlap with ASD- and schizophrenia-associated genes, and aimed to use this approach to narrow down the list for further functional analysis. We took the human ASD gene list from SFARI with category scores≤4. Among the 460 genes included in the list, 427 were converted to mouse genes and compared with the list from our proteomic analysis (Figure 4D, left). 256 of 427 were identified in the phosphoproteome data, in which 97 targets showed significant changes in phosphorylation states by Ng KD. The list of genes with phosphorylation sites are reported in Supplemental Table S4, with highlight in synaptic components and ion channels. Among the candidate genes from the 108 Loci associated with schizophrenia (6), 241 of 333 human genes from the schizophrenia dataset were converted to mouse genes. 111 of these were identified in the phosphoproteome, in which 29 targets exhibited significant changes in phosphorylation states by Ng KD (Figure 4D, right and Supplemental Table S5).

Among the proteins with significantly altered phosphorylation by Ng KD, seven targets were associated with both ASD and schizophrenia (Figure 4E). While not all of the dysfunctions of these seven genes in ASDs and schizophrenia were fully known, hypofunction of NMDARs, in certain cases, Grin2A (NR2A, GluN2A), was implicated in ASD and schizophrenia (85, 86). Additionally, Grin2A is critically involved in NMDAR-dependent plasticity (87–90), providing an incentive to determine the effect of Grin2A phosphorylation on NMDAR functions. Significant P-sites identified in Grin2A are listed in Supplemental Table S6. In particular, Grin2A S1384 was significantly hypo-phosphorylated by Ng KD, and S882/S890 was hyper-phosphorylated. In a separate sample set with independent neuron culture and proteomic processing, the hypo-phosphorylation of Grin2A S1384 was validated, and three additional sites (S1198, S1201 and S1204) were also identified as hypo-phosphorylated sites, implying the tolerance at certain phosphorylation sites. To further characterize the change in Grin2A phosphorylation by Ng KD, we used a Phos-Tag system, which separates proteins based on phosphorylation levels (64, 91), and found that Ng KD caused hypo-phosphorylation of Grin2A (Figure 4F).

C-terminal phosphorylation of Grin2A modulates NMDAR-mediated current kinetics

Grin2A-containing NMDAR is required for STDP-LTP (90), and the C-terminal region of Grin subunits regulates NMDAR channel kinetics (92–94), including the phosphorylation of Grin2A C-terminus (94–97). Given the hypo-phosphorylation of Grin2A, we examined whether the four serine sites regulate NMDAR current kinetics. We generated Grin2A mutants in which S1198/1201/1204/1384 were mutated to alanine (SA; phospho-deficient) or aspartic acid (SD; phospho-mimetic), and a C-terminal truncated mutant (–Ct) (Figure 5A). The Grin2A constructs were co-expressed with Grin1 (NR1, GluN1) separated by a self-cleaving P2A peptide in HEK cells (Figure 5A, B). Dox-induced expression of constructs was validated by qPCR, western blot, and live-cell imaging (Figure 5C and

Supplemental Figure S8A, B). The responses from mutant channels elicited by glutamate were examined using the single-cell planar patch clamp (Figure 5D) (98).

SA and SD mutants exhibited significantly faster decay of NMDAR-mediated currents compared to WT and –Ct mutant (Figure 5E-I). The decay kinetics were not correlated with the peak amplitude in all mutants (Supplemental Figure S8C, D), indicating that the difference in the decay kinetics is not due to the amount of calcium influx. This was further supported by the recording in Ba^{2+}-containing solutions, in which SA and SD mutants also exhibited significantly faster decay compared to WT and –Ct mutant (Supplemental Figure S8E-J). The accelerated current profile of the SD mutant was surprising, because it was designed to mimic the phosphorylated state at the mutated residues. It is likely that both SA and SD mutants mimic the dephosphorylated state of Grin2A at these phosphorylation sites, which does not fulfill the structural requirement of a phosphorylated serine residue to slow down the current decay. Similar results were previously observed with other proteins (99–102). We also could not exclude the possibility that both SA and SD mutants lead to other unidentified changes within the channels that contribute to the accelerated current decay.

SA and SD mutants also exhibited accelerated current rise compared to WT and –Ct channels when recorded in Ca^{2+}-based solutions (Supplemental Figure S9). This acceleration became non-significant when recordings were performed in Ba^{2+}-based solutions, implicating that the effect of phosphorylation on channel activation is calcium-dependent. Together, these results demonstrate that the phosphorylation state of Grin2A C-terminus regulates the kinetics of NMDAR currents, and the dephosphorylation of serine sites S1198/1201/1204/1384 accelerates the current rise and decay.

Decreased Ng levels accelerate the decay of synaptic NMDAR currents dependent on PP2B activity

The induction of STDP-LTP requires calcium influx through NMDARs (75–77). Given our results on hypo-phosphorylation of the Grin2A subunit by Ng KD and its functional implication (Figure 4F and Figure 5), we examined the kinetics of synaptically evoked NMDAR currents in Ng KD neurons, and found that NMDAR-mediated currents showed faster decay (Figure 6A). This is consistent with the results of SA and SD mutants in HEK cells, implicating that Ng KD caused more transient calcium influx through synaptic NMDARs by the de-phosphorylation of Grin2A.

With decreased Ng levels, more CaM becomes available for calcium binding under a resting condition, likely increasing PP2B activity due to its high affinity for Ca^{2+}/CaM (103). Therefore, we tested whether suppressing PP2B could rescue the accelerated decay of synaptic NMDAR-mediated currents using FK506, a highly specific and potent PP2B inhibitor (104–106). FK506 treatment had no effect on the decay kinetics of NMDAR currents in control neurons, but it rescued the accelerated decay in Ng KD neurons (Figure 6A). These results implicate that basal synaptic PP2B activity in control neurons, if any, does not affect the kinetics of NMDAR currents. In Ng KD, however, decreased Ng levels likely elevate synaptic PP2B activity, which in turn dephosphorylates the Grin2A subunit at synapses and accelerates the decay of NMDAR-mediated currents (95, 96).

Given the role of PP2B in regulating synaptic plasticity (41, 107, 108), we tested whether PP2B activity is required for the impaired LTP observed with Ng KD. Notably, bath application of FK506 rescued LTP in Ng KD neurons (Figure 6C-E) without affecting the magnitude of LTP in the control cells (Figure 6B, D, E). Taken together, these results implicate that decreased Ng levels impair STDP-LTP via recruiting synaptic PP2B activity.

Ng overexpression and decreased PP2B activity converge on the effect on STDP-LTP

We further examined whether the broadened temporal window for STDP-LTP by Ng OE also involves PP2B. Ng OE would suppress the formation of Ca^{2+}/CaM complexes and thus inhibit basal PP2B activity. If Ng OE decreases PP2B activity which exerts its effect on LTP, then blocking PP2B activity is likely to mimic Ng OE. In fact, bath application of FK506 enabled control cells to express STDP-LTP with the 20-ms pairing protocol which failed to induce LTP in the vehicle conditions (Figure 7A, B, E-G), implicating that basal PP2B activity restricts the timing window for STDP-LTP. Importantly, Ng OE occluded the effect of FK506 on broadening the timing window (Figure 7C-G), suggesting that Ng OE exerts the effect on STDP-LTP by suppressing PP2B activity.

Discussion

Information encoding in the brain requires long-lasting changes in excitatory synaptic strength, primarily mediated by Ca^{2+}/CaM-dependent signaling through NMDARs. Here we report that Ng controls the efficacy of this process dependent on PP2B activity.

The total concentrations of CaM-binding proteins are significantly higher than CaM itself, making CaM a limiting factor (109). In neurons, Ng further limits CaM by forming Ng-CaM complexes, where the total concentrations of Ng and CaM are estimated to be 20 and 10 μM, respectively (53, 55). Given the high binding affinity between Ng and CaM (110), the majority of CaM is thought to exist as Ng-CaM complex at the rest state (53). Ng KD likely releases CaM for calcium binding in the spine and recruits PP2B activity, causing the accelerated decay of NMDAR-mediated currents and the impaired LTP (Supplemental Figure S10A). Conversely, increasing Ng levels sequesters CaM, and thus suppresses PP2B activity (Supplemental Figure S10B). FK506 mimicked and occluded the effect of Ng OE on STDP-LTP, indicating that Ng OE broadened the timing window for LTP through inhibiting PP2B activity. Given that FK506 did not alter the decay kinetics of synaptically evoked NMDAR currents in control cells (Figure 6A), likely there is little *synaptic* PP2B activity in the control cells capable of slowing the synaptic NMDAR current decay, and the effect of Ng OE or FK506 on STDP-LTP may be due to the suppression of PP2B activity at *peri-* or *extra-synaptic* locations on different neuronal targets. Ng is localized in the dendritic spines (22, 111), and thus basal PP2B activity is presumably higher at *peri-* or *extra-synaptic* sites compared to dendritic spines.

Our proteomic analysis revealed that Ng KD has profound effect on the phosphoproteome landscape, highlighting PSD components. In particular, Ng KD altered phosphorylation patterns of ion channels and neurotransmitter receptors, suggesting a functional impact on membrane properties and synaptic inputs. We narrowed down the significant targets using the overlapping genes of Ng KD phosphoproteome, ASD and schizophrenia datasets,

given that 1) Ng is a schizophrenia-associated gene and a target in an inherited ASD, Jacobsen's Syndrome; 2) Ng KD dataset is highly enriched in PSD components, and ASD and SCZ gene sets also highlight the glutamate synaptic network. This approach is poised to provide overlap that converges the three different data sets. Whether this overlap indicates a converging pathophysiology is unknown.

Grin2A is one of the gene targets present in all three datasets, which is essential for mediating synaptic plasticity. Our results implicate that Ng KD caused NMDAR hypofunction, likely via the hypo-phosphorylation of Grin2A. The SA and SD mutants of Grin2A exhibited faster current decay, and Ng KD accelerated synaptic NMDAR current decay in a PP2B-dependent manner, consistent with previous findings that Grin2A dephosphorylation accelerates NMDAR current decay (97).

Ng KD caused significant hyper-phosphorylation of certain targets, suggesting that the effect of Ng KD on phosphoproteome is not a generic consequence of overall increase in phosphatase activities. Our functional validation of the PP2B-Grin2A pathway provides a proof of principle for analyzing functional consequence of phosphoproteome targets beyond the Ng-PP2B-Grin2A axis. While the measurement of synaptic NMDAR current kinetics reports the synaptic effect caused by Ng KD dependent on PP2B activity, it is conceivable that PP2B targets beyond Grin2A contribute to the altered temporal window of STDP, and other CaM-dependent signaling events could also be involved. In fact, our phosphoproteomic studies identified changes in phosphorylation in multiple ion channels, including L-type calcium channels and small conductance calcium-activated potassium channels, which are known to regulate STDP (75, 112) and regulated by CaM (113, 114). Moreover, neuromodulators also gate the polarity and temporal window of STDP (42), and the adrenergic receptor family was a significant hit in the phosphoproteome dataset. These are important future directions for in-depth investigation to fully decipher molecular mechanisms of STDP controlled by Ng/CaM-pathways. Moreover, whether and how Ng levels are associated with decreased hippocampal activation in schizophrenia (18) is currently unknown. Given that Ng KD caused significant changes in the phosphorylation of voltage-gated ion channels (Supplemental Tables S4, 5), it will be important to investigate how these phosphorylation events affect neuronal excitability at the circuit level.

Collectively, our data provide evidence that Ng controls the induction of LTP in the hippocampus. Ng translation is rapidly up-regulated following neuronal activity (26), and the elevated Ng levels likely facilitate LTP induction between co-activated and connected neurons, thereby establishing the engram representing specific events. Consistent with our findings in the hippocampus, Ng OE in the prefrontal cortex enhances plasticity and extinction learning (115). However, we cannot formally exclude that broadening of the timing window (decreasing timing-contingency) is disruptive, and excessively high levels of Ng under pathological conditions may cause abnormal and persistent memory association.

Our results highlight that the components in the Ca^{2+}/CaM-dependent signaling cascade, particularly the Ng-PP2B-Grin2A axis, are potential therapeutic targets for cognitive impairment associated with schizophrenia, Jacobsen syndrome and Alzheimer's disease.

Supplementary Material

Refer to Web version on PubMed Central for supplementary material.

Acknowledgements

This work was supported by the Broad Institute Stanley Center Neuropsychiatry Initiative grant, the JPB foundation, the Whitehall foundation and NIMH (MH118298, W.X.), and the Brain Research Program through the National Research Foundation of Korea (NRF) funded by the Ministry of Science, ICT & Future Planning (2016M3C7A1913845, H.R.). A preprint containing a previous version of the manuscript was posted at bioRxiv (DOI: https://doi.org/10.1101/481291).

References

1. Freedman R (2003): Schizophrenia. N Engl J Med 349:1738–1749. [PubMed: 14585943]
2. Lopez AD, Murray CC (1998): The global burden of disease, 1990–2020. Nat Med 4:1241–1243. [PubMed: 9809543]
3. Palmer BA, Pankratz VS, Bostwick JM (2005): The lifetime risk of suicide in schizophrenia: a reexamination. Arch Gen Psychiatry 62:247–253. [PubMed: 15753237]
4. Sullivan PF, Kendler KS, Neale MC (2003): Schizophrenia as a complex trait: evidence from a meta-analysis of twin studies. Arch Gen Psychiatry 60:1187–1192. [PubMed: 14662550]
5. Lichtenstein P, Bjork C, Hultman CM, Scolnick E, Sklar P, Sullivan PF (2006): Recurrence risks for schizophrenia in a Swedish national cohort. Psychol Med 36:1417–1425. [PubMed: 16863597]
6. Schizophrenia Working Group of the Psychiatric Genomics C (2014): Biological insights from 108 schizophrenia-associated genetic loci. Nature 511:421–427. [PubMed: 25056061]
7. Stefansson H, Ophoff RA, Steinberg S, Andreassen OA, Cichon S, Rujescu D, et al. (2009): Common variants conferring risk of schizophrenia. Nature, pp 744–747.
8. International Schizophrenia C, Purcell SM, Wray NR, Stone JL, Visscher PM, O'Donovan MC, et al. (2009): Common polygenic variation contributes to risk of schizophrenia and bipolar disorder. Nature 460:748–752. [PubMed: 19571811]
9. Ripke S, O'Dushlaine C, Chambert K, Moran JL, Kahler AK, Akterin S, et al. (2013): Genome-wide association analysis identifies 13 new risk loci for schizophrenia. Nat Genet 45:1150–1159. [PubMed: 23974872]
10. Ikeda M, Aleksic B, Kinoshita Y, Okochi T, Kawashima K, Kushima I, et al. (2011): Genome-wide association study of schizophrenia in a Japanese population. Biol Psychiatry 69:472–478. [PubMed: 20832056]
11. Schizophrenia Psychiatric Genome-Wide Association Study C (2011): Genome-wide association study identifies five new schizophrenia loci. Nat Genet 43:969–976. [PubMed: 21926974]
12. Shi J, Levinson DF, Duan J, Sanders AR, Zheng Y, Pe'er I, et al. (2009): Common variants on chromosome 6p22.1 are associated with schizophrenia. Nature 460:753–757. [PubMed: 19571809]
13. Yue WH, Wang HF, Sun LD, Tang FL, Liu ZH, Zhang HX, et al. (2011): Genome-wide association study identifies a susceptibility locus for schizophrenia in Han Chinese at 11p11.2. Nat Genet 43:1228–1231. [PubMed: 22037552]
14. Rietschel M, Mattheisen M, Degenhardt F, Genetic R, Outcome in P, Muhleisen TW, et al. (2012): Association between genetic variation in a region on chromosome 11 and schizophrenia in large samples from Europe. Mol Psychiatry 17:906–917. [PubMed: 21747397]
15. Ohi K, Hashimoto R, Yasuda Y, Fukumoto M, Yamamori H, Umeda-Yano S, et al. (2012): Functional genetic variation at the NRGN gene and schizophrenia: evidence from a gene-based case-control study and gene expression analysis. Am J Med Genet B Neuropsychiatr Genet 159B:405–413. [PubMed: 22461181]
16. Ohi K, Hashimoto R, Yasuda Y, Fukumoto M, Yamamori H, Umeda-Yano S, et al. (2013): Influence of the NRGN gene on intellectual ability in schizophrenia. J Hum Genet, pp 700–705. [PubMed: 23903071]

17. Ruano D, Aulchenko YS, Macedo A, Soares MJ, Valente J, Azevedo MH, et al. (2008): Association of the gene encoding neurogranin with schizophrenia in males. J Psychiatr Res, pp 125–133. [PubMed: 17140601]
18. Pohlack ST, Nees F, Ruttorf M, Witt SH, Nieratschker V, Rietschel M, et al. (2011): Risk variant for schizophrenia in the neurogranin gene impacts on hippocampus activation during contextual fear conditioning. Mol Psychiatry, pp 1072–1073. [PubMed: 21647148]
19. Ohi K, Hashimoto R, Yasuda Y, Nemoto K, Ohnishi T, Fukumoto M, et al. (2012): Impact of the genome wide supported NRGN gene on anterior cingulate morphology in schizophrenia. PLoS ONE, pp e29780. [PubMed: 22253779]
20. Broadbelt K, Ramprasaud A, Jones LB (2006): Evidence of altered neurogranin immunoreactivity in areas 9 and 32 of schizophrenic prefrontal cortex. Schizophr Res, pp 6–14. [PubMed: 16797925]
21. Krueger DD, Nairn AC (2007): Expression of PKC substrate proteins, GAP-43 and neurogranin, is downregulated by cAMP signaling and alterations in synaptic activity. Eur J Neurosci, pp 3043–3053. [PubMed: 18005072]
22. Neuner-Jehle M, Denizot JP, Mallet J (1996): Neurogranin is locally concentrated in rat cortical and hippocampal neurons. Brain Res, pp 149–154.
23. Ressler KJ, Paschall G, Zhou X-l, Davis M (2002): Regulation of synaptic plasticity genes during consolidation of fear conditioning. J Neurosci, pp 7892–7902. [PubMed: 12223542]
24. Represa A, Deloulme JC, Sensenbrenner M, Ben-Ari Y, Baudier J (1990): Neurogranin: immunocytochemical localization of a brain-specific protein kinase C substrate. J Neurosci, pp 3782–3792. [PubMed: 2269883]
25. Han KS, Cooke SF, Xu W (2017): Experience-Dependent Equilibration of AMPAR-Mediated Synaptic Transmission during the Critical Period. Cell Rep 18:892–904. [PubMed: 28122240]
26. Jones KJ, Templet S, Zemoura K, Kuzniewska B, Pena FX, Hwang H, et al. (2018): Rapid, experience-dependent translation of neurogranin enables memory encoding. Proc Natl Acad Sci U S A 115:E5805–E5814. [PubMed: 29880715]
27. Gerendasy D (1999): Homeostatic tuning of Ca2+ signal transduction by members of the calpacitin protein family. J Neurosci Res, pp 107–119.
28. Slemmon JR, Feng B, Erhardt JA (2000): Small proteins that modulate calmodulin-dependent signal transduction: effects of PEP-19, neuromodulin, and neurogranin on enzyme activation and cellular homeostasis. Mol Neurobiol: Humana Press, pp 99–113. [PubMed: 11414283]
29. Malinow R, Schulman H, Tsien RW (1989): Inhibition of postsynaptic PKC or CaMKII blocks induction but not expression of LTP. Science 245:862–866. [PubMed: 2549638]
30. Malenka RC (1994): Synaptic plasticity in the hippocampus: LTP and LTD. Cell 78:535–538. [PubMed: 8069904]
31. Nabavi S, Fox R, Proulx CD, Lin JY, Tsien RY, Malinow R (2014): Engineering a memory with LTD and LTP. Nature 511:348–352. [PubMed: 24896183]
32. Whitlock JR, Heynen AJ, Shuler MG, Bear MF (2006): Learning induces long-term potentiation in the hippocampus. Science 313:1093–1097. [PubMed: 16931756]
33. Xia Z, Storm DR (2005): The role of calmodulin as a signal integrator for synaptic plasticity. Nat Rev Neurosci 6:267–276. [PubMed: 15803158]
34. Shepherd JD, Huganir RL (2007): The cell biology of synaptic plasticity: AMPA receptor trafficking. Annu Rev Cell Dev Biol 23:613–643. [PubMed: 17506699]
35. Malenka RC, Bear MF (2004): LTP and LTD: an embarrassment of riches. Neuron 44:5–21. [PubMed: 15450156]
36. Kauer JA, Malenka RC (2007): Synaptic plasticity and addiction. Nat Rev Neurosci 8:844–858. [PubMed: 17948030]
37. Lisman JE (2001): Three Ca2+ levels affect plasticity differently: the LTP zone, the LTD zone and no man's land. J Physiol 532:285. [PubMed: 11306649]
38. Lisman J, Schulman H, Cline H (2002): The molecular basis of CaMKII function in synaptic and behavioural memory. Nat Rev Neurosci 3:175–190. [PubMed: 11994750]

39. Bayer KU, Schulman H (2019): CaM Kinase: Still Inspiring at 40. Neuron 103:380–394. [PubMed: 31394063]
40. Kennedy MB (2000): Signal-processing machines at the postsynaptic density. Science 290:750–754. [PubMed: 11052931]
41. Wang JH, Kelly PT (1996): The balance between postsynaptic Ca(2+)-dependent protein kinase and phosphatase activities controlling synaptic strength. Learn Mem 3:170–181. [PubMed: 10456087]
42. Seol GH, Ziburkus J, Huang S, Song L, Kim IT, Takamiya K, et al. (2007): Neuromodulators control the polarity of spike-timing-dependent synaptic plasticity. Neuron, pp 919–929.
43. Woolfrey KM, Dell'Acqua ML (2015): Coordination of Protein Phosphorylation and Dephosphorylation in Synaptic Plasticity. J Biol Chem 290:28604–28612. [PubMed: 26453308]
44. Ouyang Y, Rosenstein A, Kreiman G, Schuman EM, Kennedy MB (1999): Tetanic stimulation leads to increased accumulation of Ca(2+)/calmodulin-dependent protein kinase II via dendritic protein synthesis in hippocampal neurons. J Neurosci 19:7823–7833. [PubMed: 10479685]
45. De Koninck P, Schulman H (1998): Sensitivity of CaM kinase II to the frequency of Ca2+ oscillations. Science 279:227–230. [PubMed: 9422695]
46. Ouyang Y, Kantor D, Harris KM, Schuman EM, Kennedy MB (1997): Visualization of the distribution of autophosphorylated calcium/calmodulin-dependent protein kinase II after tetanic stimulation in the CA1 area of the hippocampus. J Neurosci 17:5416–5427. [PubMed: 9204925]
47. Rich RC, Schulman H (1998): Substrate-directed function of calmodulin in autophosphorylation of Ca2+/calmodulin-dependent protein kinase II. J Biol Chem 273:28424–28429. [PubMed: 9774470]
48. Miller SG, Kennedy MB (1986): Regulation of brain type II Ca2+/calmodulin-dependent protein kinase by autophosphorylation: a Ca2+-triggered molecular switch. Cell 44:861–870. [PubMed: 3006921]
49. Schulman H (2004): Activity-dependent regulation of calcium/calmodulin-dependent protein kinase II localization. J Neurosci 24:8399–8403. [PubMed: 15456811]
50. Quintana AR, Wang D, Forbes JE, Waxham MN (2005): Kinetics of calmodulin binding to calcineurin. Biochem Biophys Res Commun 334:674–680. [PubMed: 16009337]
51. Chen X, Vinade L, Leapman RD, Petersen JD, Nakagawa T, Phillips TM, et al. (2005): Mass of the postsynaptic density and enumeration of three key molecules. Proc Natl Acad Sci U S A 102:11551–11556. [PubMed: 16061821]
52. Collins MO, Husi H, Yu L, Brandon JM, Anderson CN, Blackstock WP, et al. (2006): Molecular characterization and comparison of the components and multiprotein complexes in the postsynaptic proteome. J Neurochem 97 Suppl 1:16–23. [PubMed: 16635246]
53. Zhabotinsky AM, Camp RN, Epstein IR, Lisman JE (2006): Role of the neurogranin concentrated in spines in the induction of long-term potentiation. J Neurosci: Society for Neuroscience, pp 7337–7347. [PubMed: 16837580]
54. Gerendasy DD, Sutcliffe JG (1997): RC3/neurogranin, a postsynaptic calpacitin for setting the response threshold to calcium influxes. Mol Neurobiol, pp 131–163. [PubMed: 9396008]
55. Huang K-P, Huang FL, Jäger T, Li J, Reymann KG, Balschun D (2004): Neurogranin/RC3 enhances long-term potentiation and learning by promoting calcium-mediated signaling. J Neurosci: Society for Neuroscience, pp 10660–10669. [PubMed: 15564582]
56. van Dalen JJW, Gerendasy DD, de Graan PNE, Schrama LH, Gruol DL (2003): Calcium dynamics are altered in cortical neurons lacking the calmodulin-binding protein RC3. Eur J Neurosci, pp 13–22.
57. Zhong L, Cherry T, Bies CE, Florence MA, Gerges NZ (2009): Neurogranin enhances synaptic strength through its interaction with calmodulin. EMBO J, pp 3027–3039. [PubMed: 19713936]
58. Zhong L, Gerges NZ (2012): Neurogranin targets calmodulin and lowers the threshold for the induction of long-term potentiation. PLoS ONE: Public Library of Science, pp e41275. [PubMed: 22848456]
59. Liu M, Lewis LD, Shi R, Brown EN, Xu W (2014): Differential requirement for NMDAR activity in SAP97β-mediated regulation of the number and strength of glutamatergic AMPAR-containing synapses. J Neurophysiol, pp 648–658. [PubMed: 24225540]

60. Pan JQ, Baez-Nieto D, Allen A, Wang HR, Cottrell JR (2018): Developing High-Throughput Assays to Analyze and Screen Electrophysiological Phenotypes. Methods Mol Biol 1787:235–252. [PubMed: 29736723]
61. Schluter OM, Xu W, Malenka RC (2006): Alternative N-terminal domains of PSD-95 and SAP97 govern activity-dependent regulation of synaptic AMPA receptor function. Neuron 51:99–111. [PubMed: 16815335]
62. Lois C, Hong EJ, Pease S, Brown EJ, Baltimore D (2002): Germline transmission and tissue-specific expression of transgenes delivered by lentiviral vectors. Science 295:868–872. [PubMed: 11786607]
63. Kinoshita E, Kinoshita-Kikuta E, Koike T (2009): Separation and detection of large phosphoproteins using Phos-tag SDS-PAGE. Nat Protoc: Nature Publishing Group, pp 1513–1521. [PubMed: 19798084]
64. Kinoshita E, Kinoshita-Kikuta E, Takiyama K, Koike T (2006): Phosphate-binding tag, a new tool to visualize phosphorylated proteins. Mol Cell Proteomics 5:749–757. [PubMed: 16340016]
65. Makino Y, Johnson RC, Yu Y, Takamiya K, Huganir RL (2011): Enhanced synaptic plasticity in mice with phosphomimetic mutation of the GluA1 AMPA receptor. Proc Natl Acad Sci USA: National Acad Sciences, pp 8450–8455. [PubMed: 21536866]
66. Mertins P, Qiao JW, Patel J, Udeshi ND, Clauser KR, Mani DR, et al. (2013): Integrated proteomic analysis of post-translational modifications by serial enrichment. Nat Methods 10:634–637. [PubMed: 23749302]
67. Rappsilber J, Mann M, Ishihama Y (2007): Protocol for micro-purification, enrichment, pre-fractionation and storage of peptides for proteomics using StageTips. Nat Protoc 2:1896–1906. [PubMed: 17703201]
68. Cox J, Mann M (2011): Quantitative, high-resolution proteomics for data-driven systems biology. Annu Rev Biochem 80:273–299. [PubMed: 21548781]
69. Elias JE, Gibbons FD, King OD, Roth FP, Gygi SP (2004): Intensity-based protein identification by machine learning from a library of tandem mass spectra. Nat Biotechnol 22:214–219. [PubMed: 14730315]
70. Nesvizhskii AI, Aebersold R (2005): Interpretation of shotgun proteomic data: the protein inference problem. Mol Cell Proteomics 4:1419–1440. [PubMed: 16009968]
71. Ritchie ME, Phipson B, Wu D, Hu Y, Law CW, Shi W, et al. (2015): limma powers differential expression analyses for RNA-sequencing and microarray studies. Nucleic Acids Res 43:e47. [PubMed: 25605792]
72. Smyth GK (2004): Linear models and empirical bayes methods for assessing differential expression in microarray experiments. Stat Appl Genet Mol Biol 3:Article3.
73. Bayes A, Collins MO, Croning MD, van de Lagemaat LN, Choudhary JS, Grant SG (2012): Comparative study of human and mouse postsynaptic proteomes finds high compositional conservation and abundance differences for key synaptic proteins. PLoS One 7:e46683. [PubMed: 23071613]
74. Yu G, Wang LG, Han Y, He QY (2012): clusterProfiler: an R package for comparing biological themes among gene clusters. OMICS 16:284–287. [PubMed: 22455463]
75. Magee JC, Johnston D (1997): A synaptically controlled, associative signal for Hebbian plasticity in hippocampal neurons. Science, pp 209–213. [PubMed: 8985013]
76. Markram H, Lubke J, Frotscher M, Sakmann B (1997): Regulation of synaptic efficacy by coincidence of postsynaptic APs and EPSPs. Science 275:213–215. [PubMed: 8985014]
77. Bi GQ, Poo MM (1998): Synaptic modifications in cultured hippocampal neurons: dependence on spike timing, synaptic strength, and postsynaptic cell type. J Neurosci 18:10464–10472. [PubMed: 9852584]
78. Mertins P, Mani DR, Ruggles KV, Gillette MA, Clauser KR, Wang P, et al. (2016): Proteogenomics connects somatic mutations to signalling in breast cancer. Nature 534:55–62. [PubMed: 27251275]
79. Mertins P, Yang F, Liu T, Mani DR, Petyuk VA, Gillette MA, et al. (2014): Ischemia in tumors induces early and sustained phosphorylation changes in stress kinase pathways but does not affect global protein levels. Mol Cell Proteomics 13:1690–1704. [PubMed: 24719451]

80. Kuleshov MV, Jones MR, Rouillard AD, Fernandez NF, Duan Q, Wang Z, et al. (2016): Enrichr: a comprehensive gene set enrichment analysis web server 2016 update. Nucleic Acids Res 44:W90–97. [PubMed: 27141961]
81. Chen EY, Tan CM, Kou Y, Duan Q, Wang Z, Meirelles GV, et al. (2013): Enrichr: interactive and collaborative HTML5 gene list enrichment analysis tool. BMC Bioinformatics 14:128. [PubMed: 23586463]
82. Gene Ontology C (2015): Gene Ontology Consortium: going forward. Nucleic Acids Res 43:D1049–1056. [PubMed: 25428369]
83. Ashburner M, Lewis S (2002): On ontologies for biologists: the Gene Ontology--untangling the web. Novartis Found Symp 247:66–80; discussion 80–63, 84–90, 244–252. [PubMed: 12539950]
84. Koopmans F, van Nierop P, Andres-Alonso M, Byrnes A, Cijsouw T, Coba MP, et al. (2019): SynGO: An Evidence-Based, Expert-Curated Knowledge Base for the Synapse. Neuron 103:217–234 e214. [PubMed: 31171447]
85. Tarabeux J, Kebir O, Gauthier J, Hamdan FF, Xiong L, Piton A, et al. (2011): Rare mutations in N-methyl-D-aspartate glutamate receptors in autism spectrum disorders and schizophrenia. Transl Psychiatry 1:e55. [PubMed: 22833210]
86. Voineagu I, Wang X, Johnston P, Lowe JK, Tian Y, Horvath S, et al. (2011): Transcriptomic analysis of autistic brain reveals convergent molecular pathology. Nature 474:380–384. [PubMed: 21614001]
87. Sakimura K, Kutsuwada T, Ito I, Manabe T, Takayama C, Kushiya E, et al. (1995): Reduced hippocampal LTP and spatial learning in mice lacking NMDA receptor epsilon 1 subunit. Nature 373:151–155. [PubMed: 7816096]
88. Philpot BD, Cho KK, Bear MF (2007): Obligatory role of NR2A for metaplasticity in visual cortex. Neuron 53:495–502. [PubMed: 17296552]
89. Shipton OA, Paulsen O (2014): GluN2A and GluN2B subunit-containing NMDA receptors in hippocampal plasticity. Philos Trans R Soc Lond B Biol Sci 369:20130163. [PubMed: 24298164]
90. Gerkin RC, Lau PM, Nauen DW, Wang YT, Bi GQ (2007): Modular competition driven by NMDA receptor subtypes in spike-timing-dependent plasticity. J Neurophysiol 97:2851–2862. [PubMed: 17267756]
91. Hosokawa T, Mitsushima D, Kaneko R, Hayashi Y (2015): Stoichiometry and phosphoisotypes of hippocampal AMPA-type glutamate receptor phosphorylation. Neuron 85:60–67. [PubMed: 25533481]
92. Krupp JJ, Vissel B, Thomas CG, Heinemann SF, Westbrook GL (1999): Interactions of calmodulin and alpha-actinin with the NR1 subunit modulate Ca2+-dependent inactivation of NMDA receptors. J Neurosci 19:1165–1178. [PubMed: 9952395]
93. Ehlers MD, Zhang S, Bernhadt JP, Huganir RL (1996): Inactivation of NMDA receptors by direct interaction of calmodulin with the NR1 subunit. Cell 84:745–755. [PubMed: 8625412]
94. Maki BA, Aman TK, Amico-Ruvio SA, Kussius CL, Popescu GK (2012): C-terminal domains of N-methyl-D-aspartic acid receptor modulate unitary channel conductance and gating. J Biol Chem 287:36071–36080. [PubMed: 22948148]
95. Krupp JJ, Vissel B, Thomas CG, Heinemann SF, Westbrook GL (2002): Calcineurin acts via the C-terminus of NR2A to modulate desensitization of NMDA receptors. Neuropharmacology, pp 593–602. [PubMed: 11985816]
96. Shi J, Townsend M, Constantine-Paton M (2000): Activity-dependent induction of tonic calcineurin activity mediates a rapid developmental downregulation of NMDA receptor currents. Neuron, pp 103–114. [PubMed: 11086987]
97. Townsend M, Liu Y, Constantine-Paton M (2004): Retina-driven dephosphorylation of the NR2A subunit correlates with faster NMDA receptor kinetics at developing retinocollicular synapses. J Neurosci: Society for Neuroscience, pp 11098–11107. [PubMed: 15590926]
98. Milligan CJ, Moller C (2013): Automated planar patch-clamp. Methods Mol Biol 998:171–187. [PubMed: 23529429]
99. Szczepanowska J, Ramachandran U, Herring CJ, Gruschus JM, Qin J, Korn ED, et al. (1998): Effect of mutating the regulatory phosphoserine and conserved threonine on the activity of the

expressed catalytic domain of Acanthamoeba myosin I heavy chain kinase. Proc Natl Acad Sci U S A 95:4146–4151. [PubMed: 9539704]

100. Littlepage LE, Wu H, Andresson T, Deanehan JK, Amundadottir LT, Ruderman JV (2002): Identification of phosphorylated residues that affect the activity of the mitotic kinase Aurora-A. Proc Natl Acad Sci U S A 99:15440–15445. [PubMed: 12422018]
101. Zheng W, Zhang Z, Ganguly S, Weller JL, Klein DC, Cole PA (2003): Cellular stabilization of the melatonin rhythm enzyme induced by nonhydrolyzable phosphonate incorporation. Nat Struct Biol 10:1054–1057. [PubMed: 14578935]
102. Dai H, Ding H, Meng XW, Lee SH, Schneider PA, Kaufmann SH (2013): Contribution of Bcl-2 phosphorylation to Bak binding and drug resistance. Cancer Res 73:6998–7008. [PubMed: 24097825]
103. Stefan MI, Edelstein SJ, Le Novère N (2008): An allosteric model of calmodulin explains differential activation of PP2B and CaMKII. Proc Natl Acad Sci USA: National Acad Sciences, pp 10768–10773. [PubMed: 18669651]
104. Kim D, Hwang HY, Kim JY, Lee JY, Yoo JS, Marko-Varga G, et al. (2017): FK506, an Immunosuppressive Drug, Induces Autophagy by Binding to the V-ATPase Catalytic Subunit A in Neuronal Cells. J Proteome Res 16:55–64. [PubMed: 28056508]
105. Weiwad M, Edlich F, Kilka S, Erdmann F, Jarczowski F, Dorn M, et al. (2006): Comparative analysis of calcineurin inhibition by complexes of immunosuppressive drugs with human FK506 binding proteins. Biochemistry 45:15776–15784. [PubMed: 17176100]
106. Kolos JM, Voll AM, Bauder M, Hausch F (2018): FKBP Ligands-Where We Are and Where to Go? Front Pharmacol 9:1425. [PubMed: 30568592]
107. Zeng H, Chattarji S, Barbarosie M, Rondi-Reig L, Philpot BD, Miyakawa T, et al. (2001): Forebrain-specific calcineurin knockout selectively impairs bidirectional synaptic plasticity and working/episodic-like memory. Cell 107:617–629. [PubMed: 11733061]
108. Malleret G, Haditsch U, Genoux D, Jones MW, Bliss TV, Vanhoose AM, et al. (2001): Inducible and reversible enhancement of learning, memory, and long-term potentiation by genetic inhibition of calcineurin. Cell 104:675–686. [PubMed: 11257222]
109. Persechini A, Stemmer PM (2002): Calmodulin is a limiting factor in the cell. Trends Cardiovasc Med 12:32–37. [PubMed: 11796242]
110. Huang KP, Huang FL, Li J, Schuck P, McPhie P (2000): Calcium-sensitive interaction between calmodulin and modified forms of rat brain neurogranin/RC3. Biochemistry, pp 7291–7299. [PubMed: 10852729]
111. Watson JB, Sutcliffe JG, Fisher RS (1992): Localization of the protein kinase C phosphorylation/calmodulin-binding substrate RC3 in dendritic spines of neostriatal neurons. Proc Natl Acad Sci USA, pp 8581–8585. [PubMed: 1528865]
112. Jones SL, To MS, Stuart GJ (2017): Dendritic small conductance calcium-activated potassium channels activated by action potentials suppress EPSPs and gate spike-timing dependent synaptic plasticity. Elife 6.
113. Liu X, Yang PS, Yang W, Yue DT (2010): Enzyme-inhibitor-like tuning of Ca(2+) channel connectivity with calmodulin. Nature, pp 968–972.
114. Xia XM, Fakler B, Rivard A, Wayman G, Johnson-Pais T, Keen JE, et al. (1998): Mechanism of calcium gating in small-conductance calcium-activated potassium channels. Nature 395:503–507. [PubMed: 9774106]
115. Zhong L, Brown J, Kramer A, Kaleka K, Petersen A, Krueger JN, et al. (2015): Increased prefrontal cortex neurogranin enhances plasticity and extinction learning. J Neurosci 35:7503–7508. [PubMed: 25972176]

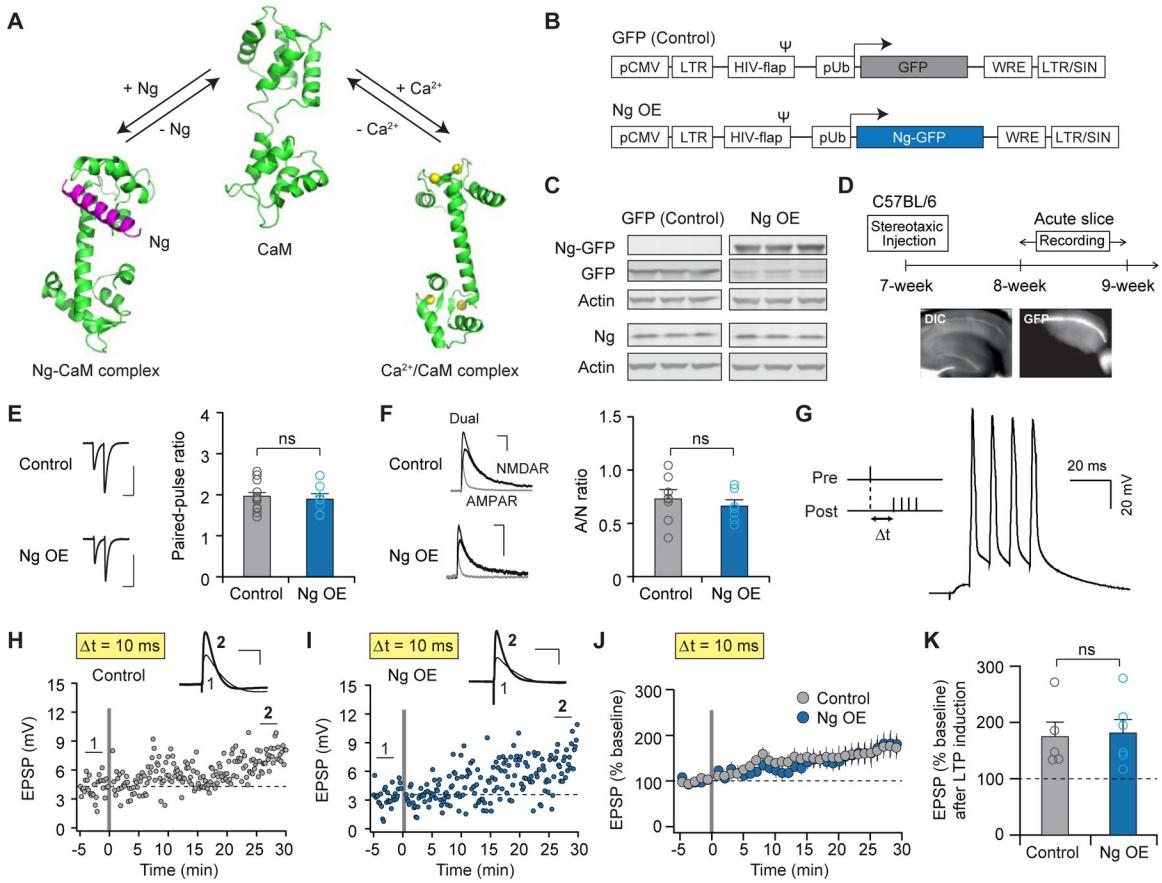

Figure 1. Ng overexpression does not affect basal synaptic transmission.

(**A**) Ng binds to CaM and regulates CaM availability. Purple: Ng (only the CaM-binding IQ motif of Ng is depicted), Green: CaM, Yellow spheres: Ca^{2+} ions (PDB: CaM, 1CFD; Ca^{2+}/CaM complex, 3CLN; Ng-CaM complex, 4E50). (**B**) Diagram of a lentivirus vector for Ng overexpression (Ng OE). LTR, long terminal repeat; Ψ, packing signal; Flap, flap element from HIV-1; pUb, ubiquitin promoter; WRE, woodchuck hepatitis virus posttranscriptional regulatory element. (**C**) Immunoblot of neuron culture infected with the Ng OE or GFP lentivirus shows overexpression of Ng-GFP or GFP, respectively. (**D**) Top: Experimental timeline for whole-cell patch clamp recordings. Bottom: The DIC and epifluorescence images display robust expression of GFP in the hippocampal CA1 region. (**E**) Paired-pulse ratio recorded at 50-ms interval from control and Ng OE neurons. Left: average traces from control and Ng OE cells (scale bars, 100 pA, 50 ms). Right: collective data of paired-pulse ratio in control (n=12 cells/10 slices/6 mice, 1.94 ± 0.10) and Ng OE (n=7/7/6, 1.89 ± 0.13) cells. The paired-pulse ratio values from individual cells are presented as open circles. The average values are presented as a bar graph with SEM (n.s.; not significant, t-test). (**F**) Comparison of NMDAR-EPSC to AMPAR-EPSC ratio in control and Ng OE neurons. Left: superimposed representative EPSC traces of dual components (compound EPSC of AMPAR and NMDAR), NMDAR-EPSC and AMPAR-EPSC measured at +40 mV. (scale bars, 50 pA, 50 ms). Right: collective data of the ratio of peak AMPAR-EPSC to NMDAR-EPSC in control (n=7/7/5, 0.73 ± 0.09) and Ng OE (n=6/6/5, 0.66 ± 0.06) cells. AMPAR/NMDAR ratio values from individual cells are presented as open circles.

The average values are presented as a bar graph with SEM (n.s.; not significant, t-test). (**G**) Left: spike-timing-dependent plasticity was induced by 100 pairings of presynaptic and postsynaptic stimulations at 5 Hz. Right: An example of current clamp recording from a CA1 neuron during the pairing. (**H, I**) Sample recordings of STDP at 10-ms pairing interval from an uninfected control cell and a cell infected with Ng OE. Gray bars indicate the timing of STDP induction. Averaged EPSP traces indicated with 1 and **2** (scale bars, 2 mV, 50 ms). (**J**) Averaged summary graphs of STDP at 10-ms interval in uninfected control (n=5) and Ng OE (n=6) cells. Each circle represents mean ± SEM. (**K**) Collective data of STDP at 10-ms interval in control (n=5/5/5, 174.7 ± 26.0%) and Ng OE (n=6/6/5, 181.4 ± 24.0%) cells. EPSP after LTP induction (% baseline) values from individual cells are presented as open circles, and the average values are presented as a bar graph with SEM (n.s.; not significant, t-test).

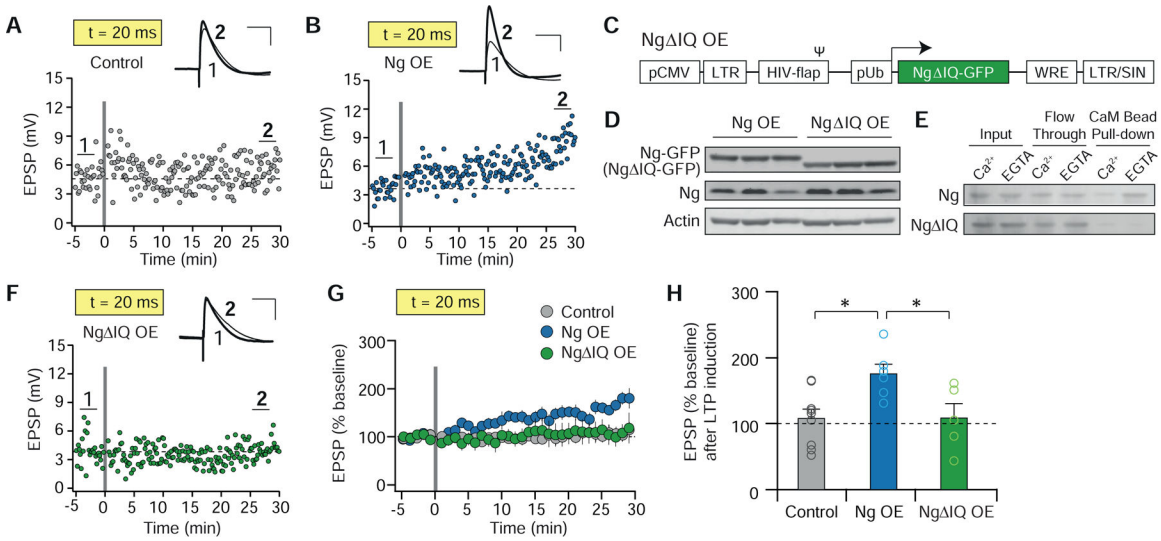

Figure 2. Ng overexpression facilitates the induction of pairing-induced LTP.

(**A, B**) Sample recordings of STDP at 20-ms pairing interval from an uninfected control cell and a cell infected with Ng OE. Gray bars indicate the timing of STDP induction. Averaged EPSP traces indicated with 1 and **2** (scale bars, 2 mV, 50 ms). (**C**) Diagram of a lentivirus vector for a Ng mutant lacking the CaM-binding IQ motif (NgΔIQ). (**D**) Immunoblot of cortical neuron culture infected with the Ng OE or the Ng deletion mutant lentivirus demonstrates effective overexpression of indicated constructs. The deletion mutant runs a bit smaller compared to the wild-type Ng, as expected. (**E**) Binding of Ng to CaM was examined by pull-down assay in the presence of 2 mM Ca^{2+} or 2 mM EGTA. Immunoblot of total cell lysate (input), flow through, and proteins bound to the CaM beads (CaM bead pull-down) samples probed with an antibody against Ng C-terminal. (**F**) A sample recording of STDP at 20-ms pairing interval from a cell infected with NgΔIQ. A gray bar indicates the timing of STDP induction. Averaged EPSP traces indicated with 1 and **2** (scale bars, 2 mV, 50 ms). (**G**) Averaged summary graphs of STDP at 20-ms interval in uninfected control (n=9), Ng OE (n=6) and NgΔIQ (n=5) cells. Each circle represents mean ± SEM. (**H**) Collective data of STDP at 20-ms interval in control (n=9/9/7, 108.2 ± 14.0%), Ng OE (n=6/6/5, 175.2 ± 14.9%) and NgΔIQ (n=5/5/4, 108.4 ± 21.9%) cells. EPSP after LTP induction (% baseline) values from individual cells are presented as open circles, and the average values are presented as a bar graph with SEM (*p<0.05, One-way ANOVA followed by Tukey's multiple comparison test).

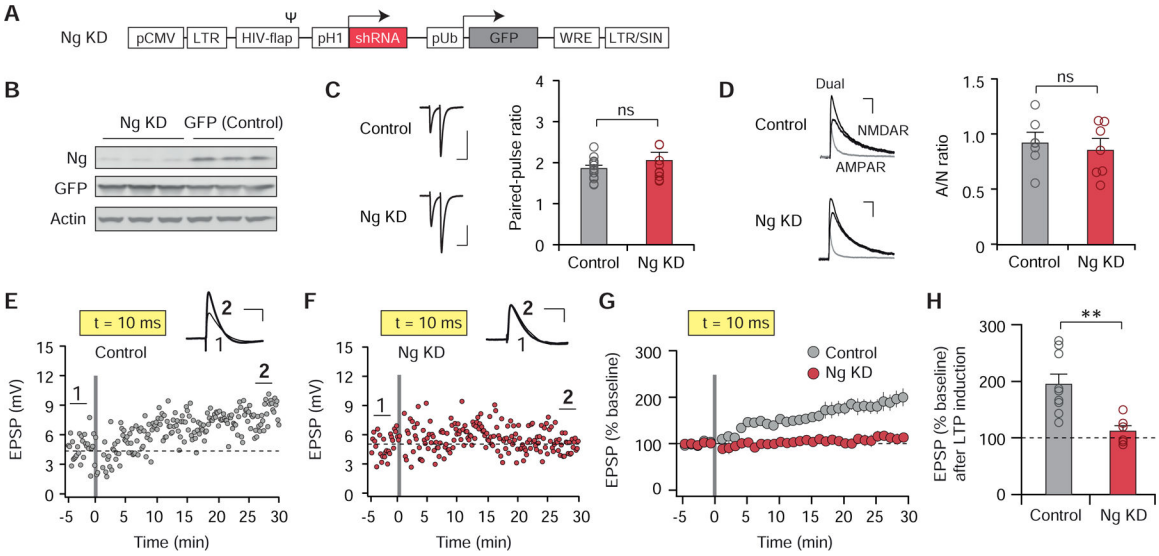

Figure 3. Ng knockdown abolishes the induction of LTP at SC-CA1 synapses.

(**A**) Diagram of a lentivirus vector for Ng knockdown (Ng KD). (**B**) Immunoblot of cortical neuron culture infected with the Ng KD or GFP only (control) lentivirus demonstrates effective knockdown of endogenous Ng. (**C**) Comparison of paired-pulse ratio at 50-ms interval recorded from control and Ng KD neurons. Left: average traces from control and Ng KD cells (scale bars, 100 pA, 50 ms). Right: collective data of paired-pulse ratio in control (n=12/9/7, 1.85 ± 0.08) and Ng KD (n=9/7/7, 2.05 ± 0.20) cells. The paired-pulse ratio values from individual cells are presented as open circles. The average values are presented as a bar graph with SEM (n.s.; not significant, t-test). (**D**) Comparison of NMDAR-EPSC to AMPAR-EPSC ratio in control and Ng KD neurons. Left: superimposed representative EPSC traces of dual components (compound EPSC of AMPAR and NMDAR), NMDAR-EPSC and AMPAR-EPSC measured at +40 mV. (scale bars, 50 pA, 50 ms). Right: collective data of the ratio of peak AMPAR-EPSC to NMDAR-EPSC in control (n=6/6/5, 0.92 ± 0.10) and Ng KD (n=7/7/5, 0.85 ± 0.11) cells. AMPAR/NMDAR ratio values from individual cells are presented as open circles. The average values are presented as a bar graph with SEM (n.s.; not significant, t-test). (**E, F**) Sample recordings of STDP at 10-ms pairing interval from an uninfected control cell and a cell infected with Ng KD. Gray bars indicate the timing of STDP induction. Averaged EPSP traces indicated with 1 and **2** (scale bars, 2 mV, 50 ms). (**G**) Averaged summary graphs of STDP at 10-ms interval in uninfected control (n=9) and Ng KD (n=6) cells. Each circle represents mean ± SEM. (**H**) Collective data of STDP at 10-ms interval in control (n=9/9/5, 194.9 ± 17.8%) and Ng KD (n=6/6/5, 112.1 ± 9.8%) cells. EPSP after LTP induction (% baseline) values from individual cells are presented as open circles, and the average values are presented as a bar graph with SEM (**p<0.01, t-test).

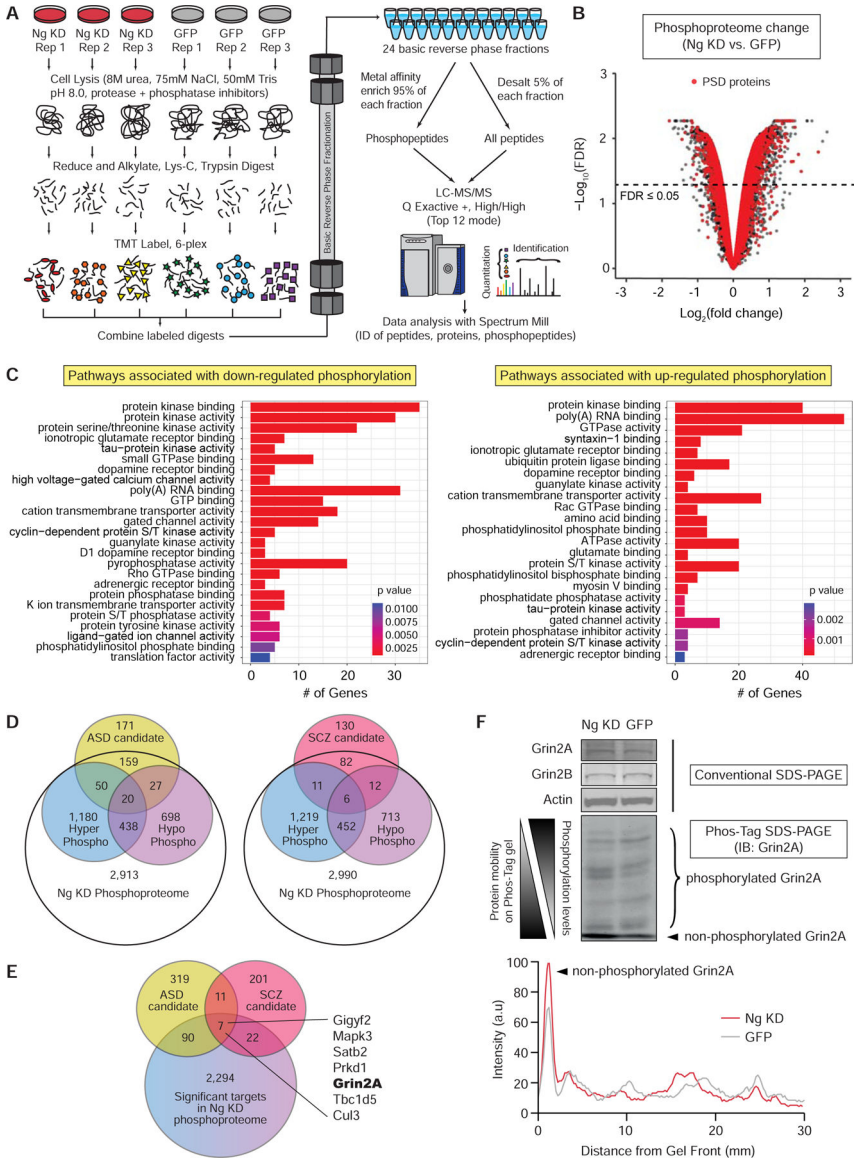

Figure 4. Knockdown of Ng causes significant shifts in neuronal phosphoproteome.

(**A**) Proteomic and phosphoproteomic workflow for the Ng KD experiment. (**B**) Volcano plots comparing the individual phosphoproteome phosphorylation sites of the Ng KD experiment. The -$\log_{10}$ of the adjusted *p* value is plotted against the average $\log_2$ fold change for the phosphoproteome. The dotted line represents an adjusted *p* value of 0.05. Red circles represent identified PSD components as described by Bayes et al (73). (**C**) Left: The pathways highlighted with down-regulated phosphorylation of PSD targets in Ng KD. Right: The pathways highlighted with up-regulated phosphorylation of PSD targets in Ng KD. (**D**) Left: The overlap of significantly affected phosphorylated targets by Ng KD with the ASD-associated gene set. Right: The overlap of significantly affected phosphorylated targets by Ng KD with the schizophrenia-associated gene set. The up-regulated phosphoproteome with Ng KD presented in blue; the down-regulated phosphoproteome with Ng KD in purple; the ASD gene set in yellow; and the schizophrenia gene set in pink. (**E**) The overlap of

significantly affected phosphorylated targets by Ng KD with both ASD- and schizophrenia-associated gene sets. (**F**) A differential phosphorylation of NMDAR subunit Grin2A was examined using a Phos-Tag SDS-PAGE, and Ng KD led to an increase in the fraction of non-phosphorylated (or least-phosphorylated) Grin2A subunit.

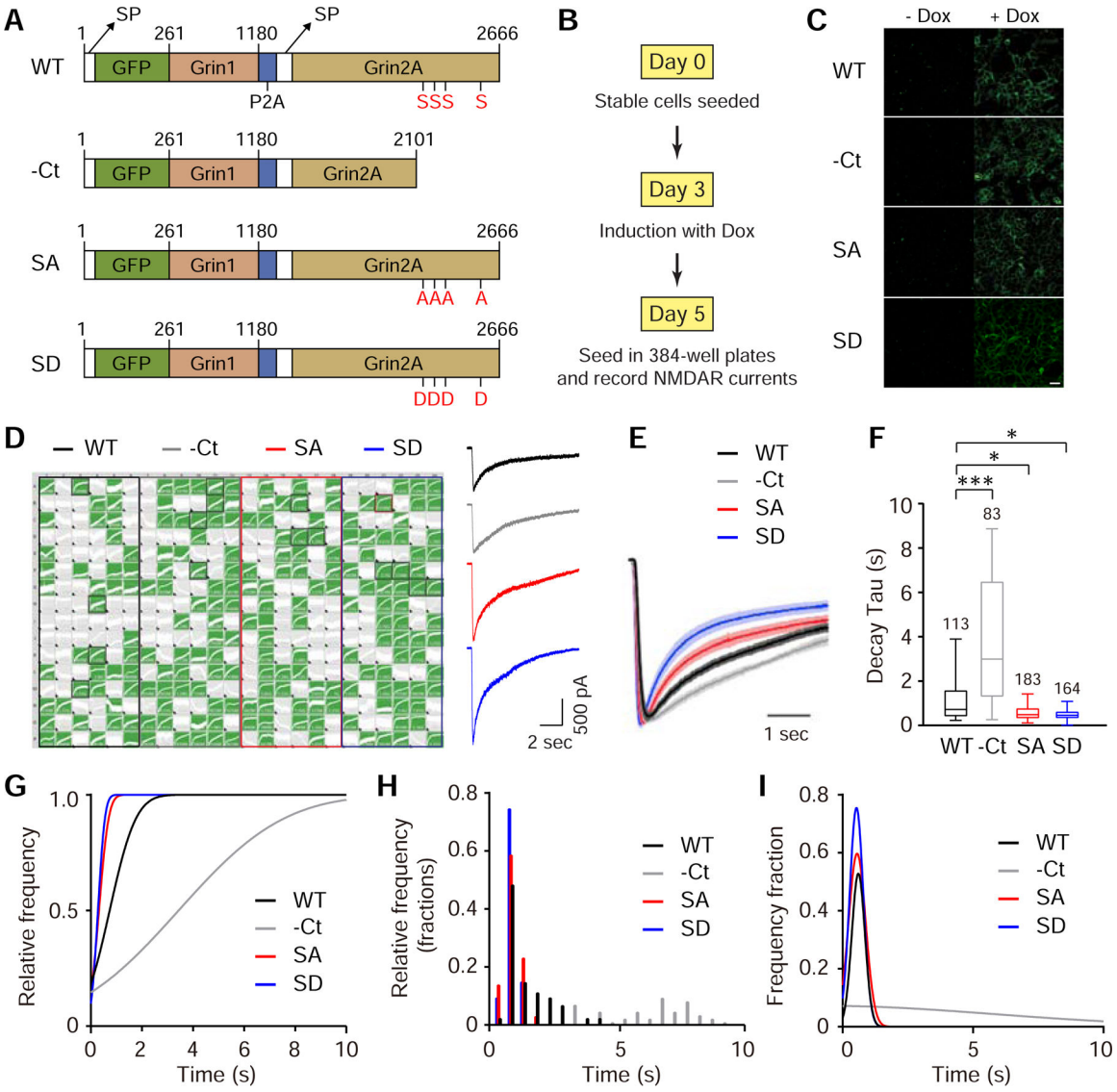

Figure 5. C-terminal phosphorylation of Grin2A modulates NMDAR-mediated current kinetics.

(**A**) Design of wild-type (WT), C-terminus deletion (–Ct), serine to alanine (SA), and serine to glutamate (SD) isogenic, single-copy, doxycycline-inducible NMDAR expression constructs. The four phosphorylation sites selected for mutation are S1198, S1201, S1204, and S1384 in rGrin2A (Uniprot ID: P35436). (**B**) Experimental design for high-throughput analysis of NMDAR-mediated currents using a 384-well planar patch clamp electrophysiology system. (**C**) Live-cell confocal images demonstrating the surface expression of NMDAR WT and mutants 48 hours post-induction with doxycycline, scale bar, 25 μm. (**D**) Left: Example of a 384-well (16 by 24) planar patch clamp recording. Right: Representative recordings of NMDAR-mediated currents using planar patch clamp. (**E**) Average traces of NMDAR currents with Grin2A WT and mutants normalized to the peak current highlight the differences in decay kinetics in –Ct, SA and SD mutants. Shaded bands represent SEM. (**F**) Box plots of decay tau values of NMDAR currents recorded from the cell lines with Grin2A WT, –Ct, SA and SD mutants. Data were compared via

one-way ANOVA and significance was calculated with the Holmes-Sidak multi-comparisons test. *p<0.05, ***p<0.001. (**G-I**) Gaussian fits of the cumulative distribution of decay kinetics (G), probability density histograms of decay kinetics (H) and its Gaussian fits (I) demonstrate Gaussian distributions for all experimental conditions except for –Ct.

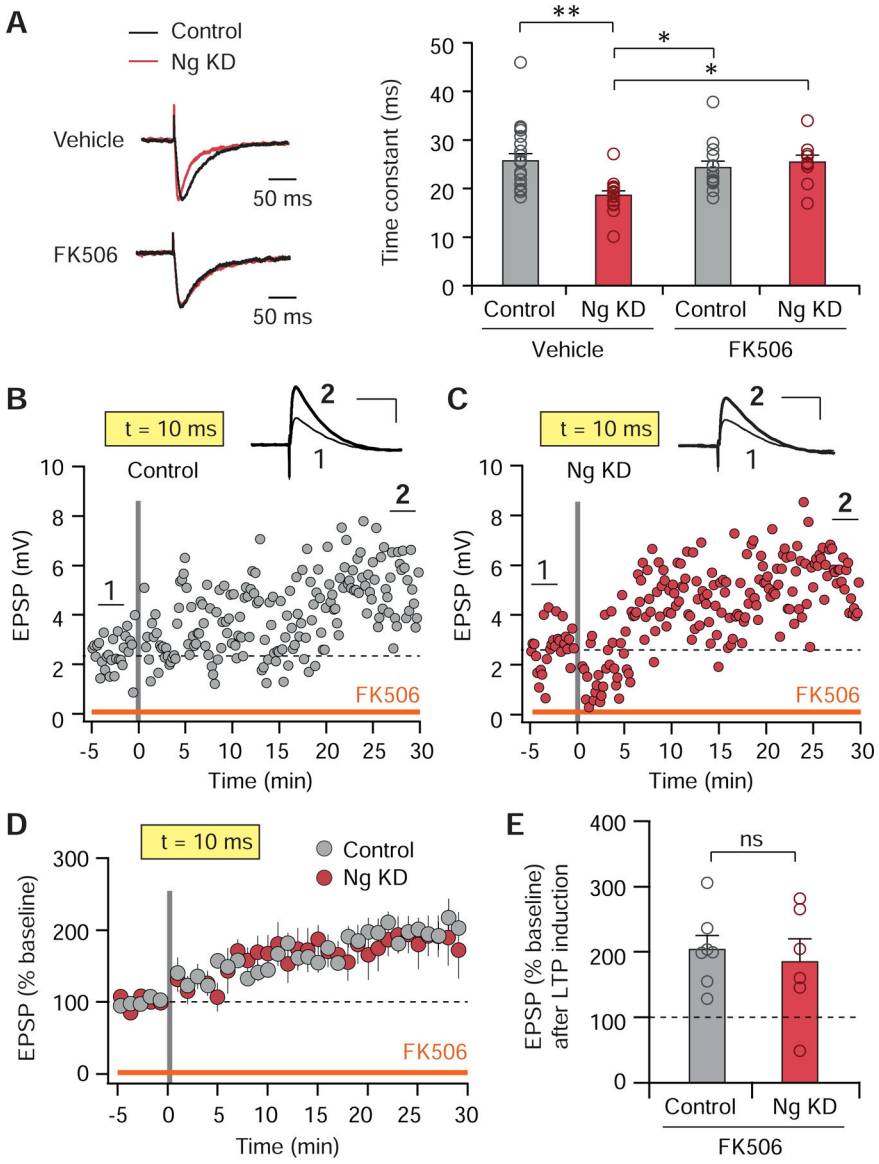

Figure 6. Ng knockdown accelerates the decay of NMDAR-mediated synaptic currents at SC-CA1 synapses by increasing PP2B activity.

(**A**) Comparison of NMDAR-mediated calcium currents recorded from control and Ng KD neurons. Left: average traces of NMDAR currents from control and Ng KD cells recorded in vehicle only (upper) or in the presence of 1 μM FK506 (bottom). NMDAR currents were fitted with a two-exponential decay function, and the slow component were not significantly different across the four conditions. Right: collective data of the fast component of NMDAR currents measured from control (n=21/17/9, 25.70 ± 1.44 ms) and Ng KD (n=15/12/9, 18.63 ± 0.92 ms) cells in vehicle and from control (n=14/10/6, 24.31 ± 1.34 ms) and Ng KD (n=10/7/6, 25.48 ± 1.41 ms) cells in FK506. The fast component of exponential decay values from individual cells are presented as open circles. The average values are presented as a bar graph with SEM (**p<0.01, *p<0.05, Two-way ANOVA followed by Tukey's multiple comparison test). (**B, C**) Sample recordings of STDP at 10-ms pairing interval from an uninfected control cell and a cell infected with Ng KD in the presence of FK506. Gray

bars indicate the timing of STDP induction. Averaged EPSP traces indicated with 1 and **2** (scale bars, 2 mV, 50 ms). The slice was treated with 1 μM FK506 for 30 min prior to the recording, and throughout the experiment. (**D**) Averaged summary graphs of STDP at 10-ms interval in uninfected control (n=7) and Ng KD (n=6) cells in the presence of FK506. Each circle represents mean ± SEM. (**E**) Collective data of STDP at 10-ms interval in control (n=7/7/6, 203.9 ± 21.6%) and Ng KD (n=6/6/6, 184.6 ± 35.1%) cells in the presence of FK506. EPSP after LTP induction (% baseline) values from individual cells are presented as open circles, and the average values are presented as a bar graph with SEM (n.s.; not significant, t-test).

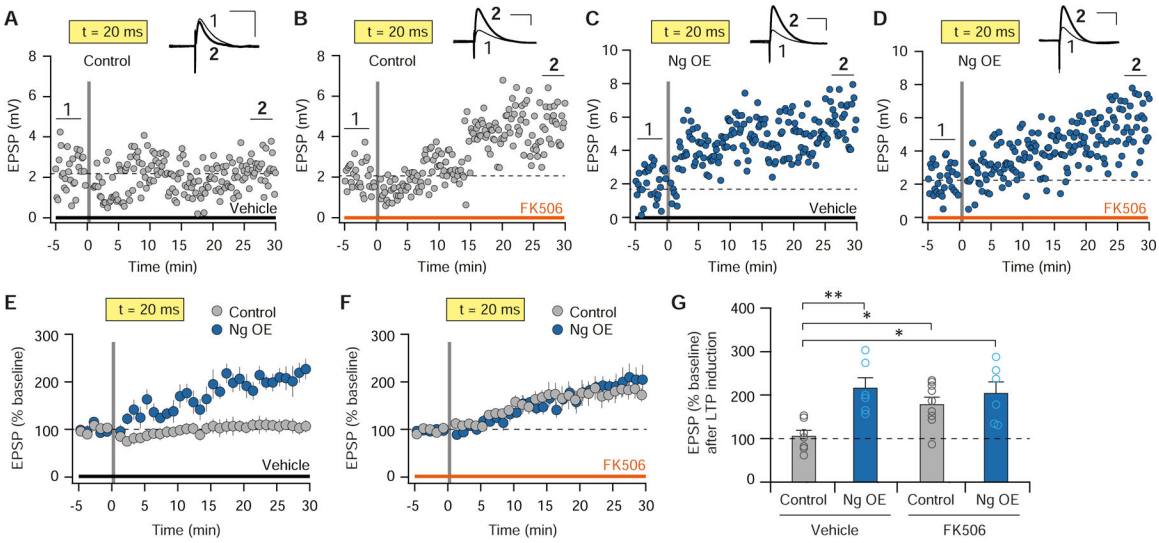

Figure 7. Ng overexpression facilitates LTP by suppressing PP2B activity.

(**A-D**) Sample recordings of STDP at 20-ms pairing interval from an uninfected control cell in vehicle only, a control cell in the presence of FK506, a cell infected with Ng OE in vehicle only, and a cell infected with Ng OE in the presence of FK506. Gray bars indicate the timing of STDP induction. Averaged EPSP traces indicated with 1 and **2** (scale bars, 2 mV, 50 ms). The slice was treated with 1 μM FK506 for 30 min prior to the recording, and throughout the experiment. (**E**) Averaged summary graphs of STDP at 20-ms interval in uninfected control cells (n=7) and Ng OE cells in vehicle (n=6). Each circle represents mean ± SEM. (**F**) Averaged summary graphs of STDP at 20-ms interval in uninfected control cells (n=9) and Ng OE cells in FK506 (n=6). Each circle represents mean ± SEM. (**G**) Collective data of STDP at 20-ms interval in control cells in vehicle (n=7/7/6, 105.7 ± 13.3%), control cells in FK506 (n=9/9/5, 179.1 ± 16.3%), Ng OE cells in vehicle (n=6/6/6, 215.6 ± 24.4%), and Ng OE cells in FK506 (n=6/6/5, 204.0 ± 26.9%). EPSP after LTP induction (% baseline) values from individual cells are presented as open circles, and the average values are presented as a bar graph with SEM (**p<0.01, *p<0.05, Two-way ANOVA followed by Tukey's multiple comparison test).

KEY RESOURCES TABLE

Resource Type	Specific Reagent or Resource	Source or Reference	Identifiers	Additional Information
Add additional rows as needed for each resource type	Include species and sex when applicable.	Include name of manufacturer, company, repository, individual, or research lab. Include PMID or DOI for references; use "this paper" if new.	Include catalog numbers, stock numbers, database IDs or accession numbers, and/or RRIDs. RRIDs are highly encouraged; search for RRIDs at https://scicrunch.org/resources.	Include any additional information or notes if necessary.
Antibody	Rabbit polyclonal anti-neurogranin	Millipore	Cat #: AB5620, RRID: AB_91937	
Antibody	Mouse monoclonal anti-β-Actin	Sigma	Cat #: A2228, A5441, RRID: AB_476697, RRID: AB_476744	
Antibody	Rabbit monoclonal anti-Grin1	Abcam	Cat #: ab109182, RRID: AB_10862307	
Antibody	Rabbit polyclonal anti-Grin2A	Millipore	Cat #: 07–632, RRID: AB_310837	
Antibody	Rabbit monoclonal anti-Grin2A	Millipore	Cat #: 05–901R, RRID: AB_10805961	
Antibody	Rabbit polyclonal anti-Grin2A	GeneTex	Cat #: GTX103558, RRID: AB_10727703	
Antibody	Rabbit polyclonal anti-NR2B	Millipore	Cat #: 06–600, RRID: AB_310193	
Antibody	Mouse monoclonal anti-CaMKIIα	Millipore	Cat #: 05–532, RRID: AB_309787	
Antibody	Mouse monoclonal anti-calcineurin (α subunit)	Sigma	Cat #: C1956, RRID: AB_258774	
Antibody	Mouse monoclonal anti-calcineurin (β subunit)	Sigma	Cat #: C0581, RRID: AB_258693	
Antibody	Mouse monoclonal anti-α-Tubulin	Sigma	Cat #: T5168, RRID: AB_477579	
Antibody	Rabbit polyclonal anti-CaMKII (phospho T286)	Abcam	Cat #: ab32678, RRID: AB_725893	
Antibody	Mouse monoclonal anti-calmodulin	Millipore	Cat #: 05–173, RRID: AB_309644	
Antibody	Rabbit polyclonal anti-GFP	Abcam	Cat #: ab6556, RRID: AB_305564	
Cell Line	Human: HEK 293T cells	ATCC	Cat #: CRL-3216, RRID: CVCL_0063	
Cell Line	Human: Flp-In™ T-REx™ 293 cells	Thermo	Cat #: R78007	
Chemical Compound or Drug	Phos-tag (TM) Acrylamide AAL-107 5mM Aqueous Solution	Wako	Cat #: 304–93526	
Chemical Compound or Drug	Calmodulin Sepharose 4B	GE Healthcare	Cat #: 17–0529-01	

Resource Type	Specific Reagent or Resource	Source or Reference	Identifiers	Additional Information
Chemical Compound or Drug	TMT-6 isobaric mass tag reagent	Thermo	Cat #: 90061	
Chemical Compound or Drug	FK506	Tocris	Cat #: 3631	
Chemical Compound or Drug	D-AP5	Tocris	Cat #: 0106	
Commercial Assay Or Kit	RNeasy Plus kit	Qiagen	Cat #: 74134	
Commercial Assay Or Kit	Pierce BCA assay kit	Thermo	Cat #: 23225	
Organism/Strain	Mouse: C57BL/6 wild-type	Charles River	N/A	
Recombinant DNA	Plasmid: FU_eGFP_GW	PMID: 16815335	N/A	
Recombinant DNA	Plasmid: FHU_eGFP_GW	PMID: 16815335	N/A	
Recombinant DNA	Plasmid: FU_Ng-eGFP_GW	This paper	N/A	
Recombinant DNA	Plasmid: FU_NgΔIQ-eGFP_GW	This paper	N/A	
Recombinant DNA	Plasmid: FH_shNg_U_eGFP_GW	This paper	N/A	
Recombinant DNA	Plasmid: pOG44	Thermo	Cat #: V600520	
Recombinant DNA	Plasmid: pFRT-TO	Thermo	Cat # V652020	
Sequence-Based Reagent	shRNA targeting sequence: neurogranin: GTGACAAGACTTCCCTACTGTTT	This paper	N/A	
Sequence-Based Reagent	Primer: rat Grin1 Forward: gtcatcatcctttctgcaagc	This paper	N/A	
Sequence-Based Reagent	Primer: rat Grin1 Reverse: ccagagatctcgcgttcc	This paper	N/A	
Sequence-Based Reagent	Primer: rat Grin2A Forward: caaggccagctgctatgg	This paper	N/A	
Sequence-Based Reagent	Primer: rat Grin2A Reverse: tgccatcccaagtcacatt	This paper	N/A	
Sequence-Based Reagent	Primer: β-Actin Forward: CCAACCGCGAGAAGATGA	Universal ProbeLibrary (Roche)	N/A	
Sequence-Based Reagent	Primer: β-Actin Reverse: CCAGAGGCGTACAGGGATAG	Universal ProbeLibrary (Roche)	N/A	
Software; Algorithm	Igor Pro 7.01	WaveMetrics	RRID: SCR_000325	https://www.wavemetrics.com/products/igorpro
Software; Algorithm	OriginPro	OriginLab	RRID: SCR_014212	https://www.originlab.com/
Software; Algorithm	GraphPad Prism 7	GraphPad Software	RRID: SCR_002798	https://www.graphpad.com/

Resource Type	Specific Reagent or Resource	Source or Reference	Identifiers	Additional Information
Software; Algorithm	Clampfit 10.5	Molecular Devices	RRID: SCR_011323	https://www.moleculardevices.com/
Software; Algorithm	FIJI (Image J 1.51h)	NIH	RRID: SCR_003070	https://imagej.nih.gov/ij/